An aerosol-mediated magnetic colloid: Study of nickel nanoparticles

Y. Sahoo
Department of Chemistry, The University at Buffalo, The State University of New York, Buffalo, New York 14260
and Institute for Lasers, Photonics and Biophotonics, The University at Buffalo, The State University of New York, Buffalo, New York 14260

Y. He and M. T. Swihart
Department of Chemical and Biological Engineering, The University at Buffalo, The State University of New York, Buffalo, New York 14260
and Institute for Lasers, Photonics and Biophotonics, The University at Buffalo, The State University of New York, Buffalo, New York 14260

S. Wang
Department of Physics, The University at Buffalo, The State University of New York, Buffalo, New York 14260

H. Luo
Department of Physics, The University at Buffalo, The State University of New York, Buffalo, New York 14260
and Institute for Lasers, Photonics and Biophotonics, The University at Buffalo, The State University of New York, Buffalo, New York 14260

E. P. Furlani
Institute for Lasers, Photonics and Biophotonics, The University at Buffalo, The State University of New York, Buffalo, New York 14260

P. N. Prasad[a)]
Department of Chemistry, The University at Buffalo, The State University of New York, Buffalo, New York 14260, Department of Physics, The University at Buffalo, The State University of New York, Buffalo, New York 14260,
and Institute for Lasers, Photonics and Biophotonics, The University at Buffalo, The State University of New York, Buffalo, New York 14260

A method is presented for the synthesis of high-quality nickel nanoparticles. Laser-driven decomposition of nickel carbonyl vapors is used to produce particles in the form of an aerosol, followed by exposure to a solvent containing an appropriate surfactant to yield a stable dispersion of particles. This method is scalable and yields a substantially monodisperse distribution of particles at a relatively high rate of production. The particles produced by this method are subjected to a detailed characterization using transmission electron microscopy, atomic force microscopy, energy dispersive spectroscopy, and dc magnetization. They have an average diameter of 5 nm, and the observed magnetization curves show no hysteresis above 200 K. The normalized magnetization curves follow a scaling law proportional to the quotient of the applied field over temperature. This data indicates the presence of randomly oriented superparamagnetic particles. The measured magnetization is significantly smaller than that of the bulk, probably due to an effective surface anisotropy and spin canting. The coercivity is the same in either direction of the applied field which indicates that there is negligible exchange coupling between the nickel particles and any possible antiferromagnetic oxide layer on their surfaces. © *2005 American Institute of Physics.*
[DOI: 10.1063/1.2033145]

I. INTRODUCTION

There is an intense and growing interest in the development of nanostructured magnetic materials, motivated primarily by the immense potential of these materials in a broad range of applications including data storage, spintronics, biomedicine, and telecommunications.[1–4] The synthesis and characterization of such materials are also important for basic science in that they can provide insight into the fundamentals of surface chemistry and magnetic interactions at the nanoscale. Magnetism in the transition elements has been investigated for decades, with the ferromagnetic series—Fe, Co, and Ni—being by far the most extensively studied systems. One fascinating discovery, surface-enhanced magnetism, in which the magnetic moments of small clusters of the ferromagnetic series exceeded their bulk values, occurred in the last decade.[5,6] These magnetic moments, in fact, exhibited dramatically higher values at a certain magic number of atoms. Ever since this discovery, an extraordinary amount of attention has been devoted to understanding the dependence

---

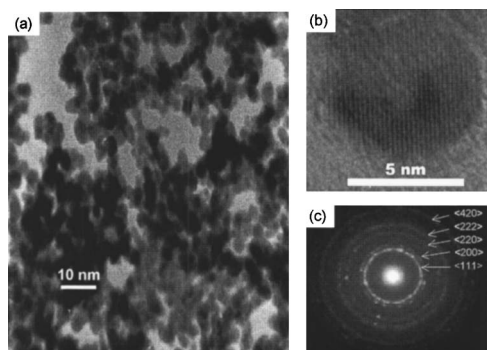a)Electronic mail: pnprasad@buffalo.edu

98, 054308-1

FIG. 1. (a) TEM image of nickel particles deposited from a toluene dispersion, (b) HRTEM image showing lattice fringes of a single particle, and (c) electron-diffraction pattern from a selected area on the TEM grid.

FIG. 2. (Color online) AFM picture of Ni particles drop cast from a pyridine dispersion onto a silicon wafer.

of magnetic properties on particle size and surface treatment. In the development of nanostructured magnetic materials, it is important to control the structure, size, composition, surface characteristics, and self-assembly of the nanoparticles, and to understand how these properties impact the bulk magnetic behavior.

The magnetic behavior of a material depends on numerous factors including the sizes, shapes, and orientations of grains within it, the structure of the grain boundaries, the magnitude and direction of internal stress, the crystallographic phases, the concomitant presence of any other phase, and the overall size and shape of the specimen.[7] All of these factors can be affected by the particle synthesis procedure. Thus, different methods of preparation are expected to result in different overall properties. This is especially true in nanomaterials because of their high surface-to-volume ratios. Over the years, a variety of procedures have been developed for the preparation of nanomagnetic materials, including hot colloidal synthesis,[8] microemulsion,[9] sol gel,[10] laser ablation,[11] and mechanical milling.[12] Each of these has advantages and disadvantages relative to the key criteria of controlling particle size, shape, dispersibility in desired solvents, yield, production rate, and processability. It is universally agreed upon that a stable dispersion of uniformly sized particles is desirable for many purposes.

In this study, the advantages of high purity and high throughput achieved in aerosol synthesis are combined with stabilization by surface treatment, as used in colloidal chemistry, to obtain a reasonably stable dispersion of nickel nanoparticles. The aerosol method adopted here is clean in that there are no side products that could adhere to the surface of the particles. Thus, the particles are devoid of any magnetic dead layers, which may be detrimental to the magnetic properties.

II. EXPERIMENT

The method of producing Ni colloid from the initial aerosol has been detailed elsewhere.[13] In short, $Ni(CO)_4$ vapor, generated by flowing CO through a bed of nickel powder, is mixed with helium and ethylene and flows into the reactor through the center of a concentric dual inlet nozzle, surrounded by a flow of helium. A CO_2 laser (Coherent, Model 42 laser emitting up to 60 W) is focused onto the
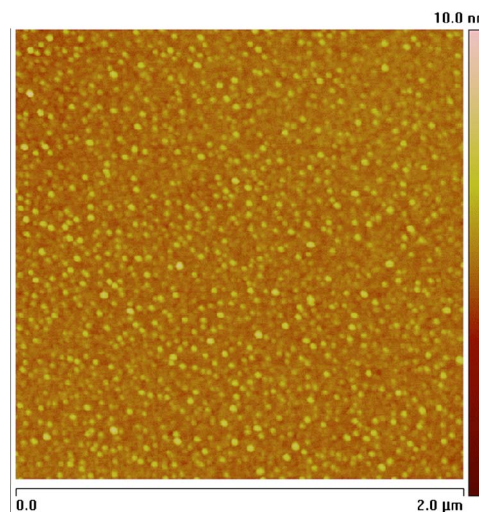
flowing mixture. The laser energy is absorbed by ethylene, which serves as a photosensitizer, resulting in very rapid heating and decomposition of $Ni(CO)_4$. Since the surrounding flow of helium is unheated, the hot gas rapidly cools by mixing with this unheated gas, quenching particle growth after a few milliseconds. The Ni particles are collected on cellulose nitrate membrane filters. The collection filters are opened in a nitrogen glove box to prevent rapid oxidation of the nickel nanopowders. The particles are dispersed in toluene, using oleic acid (97%, Aldrich) as a surfactant. Ultrasonication is used to aid in dispersion of the particles.

Transmission electron microscopy (TEM) was performed on a JEOL JEM 2010 microscope at an acceleration voltage of 200 kV. Samples were prepared for imaging by casting a drop of the toluene dispersion onto a carbon-coated TEM grid. Selected-area electron diffraction (SAED) was performed in the TEM to determine the crystalline structure of the particles. Atomic force microscopy (AFM) was performed in tapping mode on a Dimension 3100 AFM (Digital Instruments, Veeco Metrology Group, Santa Barbara, CA). Imaging was done with Veeco NanoProbe Tips model #RTESP14 with resonant frequencies of 210–280 kHz and amplitude set point of 1.4–1.6 V. Wide-angle powder x-ray diffraction was done on a Siemens D500 using the Cu $K\alpha$ line as the x-ray source. The 2θ angles ramped were from 20° to 90° to cover all the major peaks expected from nickel. Energy dispersive x-ray spectroscopy (EDAX) was obtained with a Hitachi S-4000 field-emission scanning electron microscope operating at an acceleration voltage of 20 kV. The sample was cast as a thin film from the dispersion or simply analyzed as a powder on a silicon or graphite substrate. The x-ray fluorescence beams were collected with an x-ray collection unit IXRF 500 system. Magnetization measurements (dc) were made using a superconducting quantum interference device (SQUID) MPMS C-151 magnetometer from Quantum Design Corporation. Magnetization hysteresis scans were recorded with a dc magnetic field ramped to 2 T in both directions.
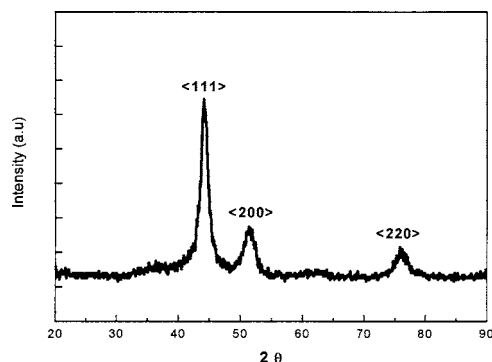
FIG. 3. XRD pattern of nickel nanoparticle powder. No phases other than metallic nickel are apparent from the diffractogram.

III. RESULTS AND DISCUSSION

The Ni nanoparticles generated here by laser pyrolysis of $Ni(CO)_4$ are spherical with an average diameter of 5 nm as indicated in the bright field TEM image in Fig. 1(a) and the AFM image in Fig. 2. The particles, treated with surfactants such as oleic acid or oleyl amine, can form a clear dispersion in nonpolar solvents like hexane and toluene. These dispersions are found to be stable without sedimentation for at least several days. The particles also form clear dispersions in pyridine, which acts as a coordinating solvent, without the need of any additional surfactant. As shown in the TEM image, the particles tend to agglomerate as the solvent evaporates from the TEM grid and they self-assemble. This may be due to strong dipolar interactions between the particles. The high-resolution transmission electron microscopy (HRTEM) shows clear lattice fringes [Fig. 1(b)]. The SAED pattern clearly shows diffraction rings that can be identified with the lattice planes of the Ni crystal [Fig. 1(c)]. The concentric rings ⟨111⟩, ⟨200⟩, ⟨220⟩, ⟨222⟩, ⟨420⟩, ⟨333,511⟩, and ⟨442⟩ bear the radii ratios 1, 1.15, 1.68, 2.0, 2.63, 2.96, and 3.48, respectively, very close to the theoretical values,[14] suggesting that the fcc lattice of the bulk Ni is well maintained at this particle size.

The crystallinity of the particles is corroborated by a clean x-ray-diffraction (XRD) pattern with peaks at 2θ values of 44.09°, 51.70°, and 76.09° that are associated with the ⟨111⟩, ⟨200⟩, and ⟨220⟩ lattice planes of nickel, respectively (Fig. 3). The presence of nickel oxide phases cannot be ruled out because the position of nickel ⟨111⟩ coincides with the strongest peak from nickel oxide, and hence there could be contribution from such a phase. But the absence of any distinguishable peak at other characteristic positions such as
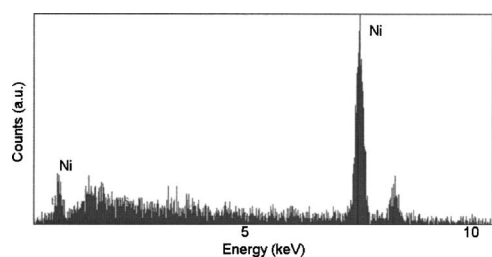

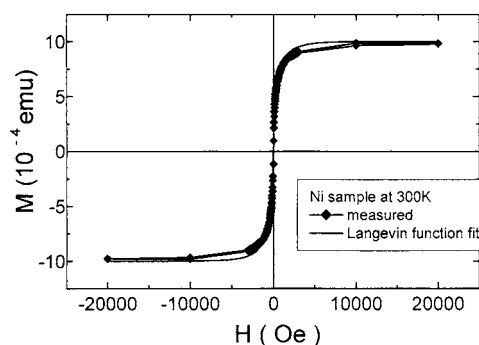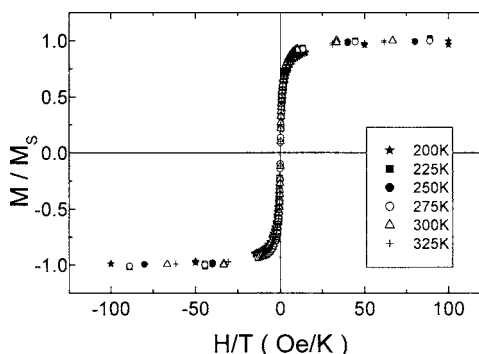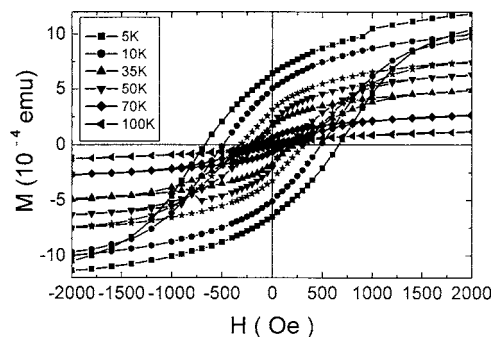
FIG. 4. EDS spectrum of nickel powder.

FIG. 5. Magnetization of nickel nanoparticles: (a) low-temperature results showing magnetic hysteresis, (b) higher-temperature results showing superparamagnetic behavior above 200 K, and (c) Langevin function fit of the magnetization curve at 300 K. The normalized plot in (b) shows the expected scaling behavior.

$2\theta=37°$, expected for nickel oxide, indicates that the presence of an oxide phase is insignificant. The Ni lattice constant is calculated using the Rietveld Analysis program[15] DBWS-9807 and found to be 3.546 Å, 0.4% larger than the bulk value of 3.532 Å. This is consistent with the general trend of lattice expansion in small nanocrystallites.[16] The average particle size estimated from all of the XRD peaks using the Scherrer formula is 4.9 nm, which is in good agreement with the AFM and TEM images.

The magnetization curves taken at different temperatures are shown in Figs. 5(a) and 5(b). No hysteresis is observed at temperatures above 200 K indicating that the particles are superparamagnetic in this range. As the sample is cooled, hysteresis curves systematically develop and widen, approaching a coercivity of 640 Oe at the lowest temperature of 5 K. The temperature dependence of the zero-field cooling (ZFC) and field cooling (FC) curves taken at an applied field of 400 Oe are shown in Fig. 6. These data show a rounding up of the ZFC curve at ∼200 K, which correlates with the

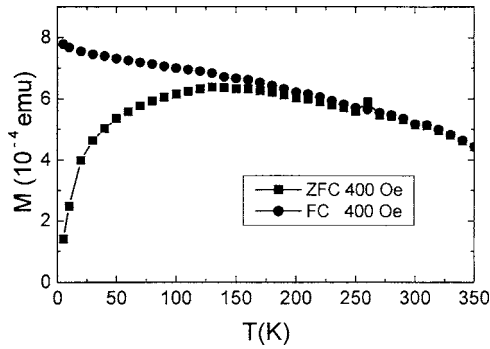FIG. 6. ZFC and FC magnetization curves for nickel nanoparticles. The onset of divergence occurs at ~150 K indicating spin blocking.

FIG. 7. Shifting of the broad maximum in the blocking curve with the applied field magnitude.

onset of superparamagnetism. In the superparamagnetic phase, the magnetization curves for an isotropic sample scale with temperature such that M/M_s plotted against H/T superimpose over each other. This scaling law is followed with minor deviation ($\leq 10\%$) probably due to interparticle interaction, in the temperature range of 200–325 K [Fig. 5(b)], emphasizing their superparamagnetic character.

The Langevin function for a classical Heisenberg spin under the influence of a field H is used to determine the effective magnetic moment μ per particle, i.e., $M/M_s = L(a) = \coth(a) - (1/a)$, where $a = \mu H/kT$ and $\mu = M_s V_{avg}$ is the particle magnetic moment. The fitting of the Langevin function to the superparamagnetic curves is shown in Fig. 5(c). By extrapolating the high-field end of the magnetization curve and normalizing for the total particle mass in the 300-K data, the saturation magnetization was found to be 31.40 emu/g as compared to a bulk value of 55.0 emu/g. The observed value translates into an effective magnetic moment of 1866 μ_B per particle, which is calculated using an average particle diameter of 5 nm and a bulk density for Ni of 8.9 g/cm^3. The lower value of saturation magnetization can arise from factors such as lattice defects that depend on the fast kinetics of $Ni(CO)_4$ decomposition, nanoparticle nucleation, and crystallization that occur on a time scale of milliseconds during particle synthesis. The surface anisotropy and spin canting in the particles also usually contribute to the decrease in the total magnetization.[17,18]

It is noteworthy that the coercivities of the magnetization curves have the same magnitude in either direction of the applied field [Fig. 5(a)]. If the surface of the Ni particles had a NiO coating layer with an appreciable thickness, then the particles could be viewed as ferromagnet-antiferromagnet core-shell structures. If the oxide coating is very thin, it will have a negligible impact on the magnetization, as was observed in Co nanoparticles with a thin CoO shell embedded in nonmagnetic matrix.[19] On the other hand, for thicker coatings the exchange coupling at the core-shell interface could result in a shift of the hysteresis loop along the field axis when the system is cooled below the Néel temperature of the antiferromagnetic phase. Previous studies have found exchange bias fields (asymmetry in the coercive fields) on the order of 700 Oe in partially oxidized Ni particles.[20] In NiO particles, Kodama *et al.* discovered large loop shifts (>10 kOe) which were attributed to a weak coupling be-
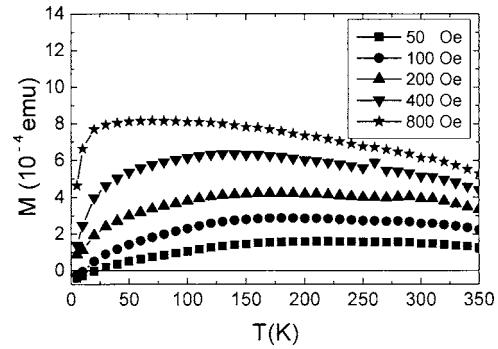
tween antiferromagnetic sublattices.[21] Our findings closely resemble those of Fonseca *et al.* in which no exchange-coupled behavior was observed when Ni particles were formed in a silica matrix through a sol-gel method.[22] Thus, this data suggests that the sample in our measurement is devoid of any significant oxide coating, probably because the particles are prepared and then dispersed into a surfactant-containing solution in an oxygen-free environment, and the surfactant may provide some protection against subsequent oxide formation.

The ZFC and FC curves, measured at a bias field of 400 Oe, overlap at temperatures above 200 K as shown in Fig. 6. Moreover, no hysteresis is observed above this temperature. The FC curve shows a steady decrease with the rise of temperature, expected from progressive randomization of the particle magnetic moments as the anisotropy barriers are overcome thermally. The ZFC curve exhibits a broad cusp implying a distribution of blocking temperatures. The blocking temperatures systematically decrease as the bias field is increased from 50 to 800 G in Fig. 7.

The blocking temperature T_B in the ZFC curve depends on various factors including the size of the nanoparticles and their intrinsic magnetic anisotropy, as well as interparticle interactions. In a recent publication, Kechrakos and Trohidou[23] have observed an increase in T_B derived from the ZFC curve of a dense dispersion of ferromagnetic particles, and attributed it to the anisotropic and ferromagnetic character of the dipolar interaction. Also, Liu and Zhang[24] have shown systematic changes in T_B with variation in size of the nanoparticles.

In our study, the broadness in the ZFC curve, which reflects a distribution of blocking temperatures, is most likely due to interactions between particles. The blocking temperature T_B is defined as the temperature that renders a magnetic relaxation time of $\tau = 10^2$ s. As discussed by Dormann *et al.*, the relaxation time τ for a superparamagnetic particle is given by the modified Brown formula,[25]

$$\tau = \tau_0 \exp\left[\frac{(E_B)}{kT}\right], \tag{1}$$

where $E_B = E_{Ba} + E_{Bint}$; $E_{Ba} = KV$ is the energy barrier of the individual particles and E_{Bint} is the additional barrier due to interactions. Here, K is the anisotropy constant and V is the
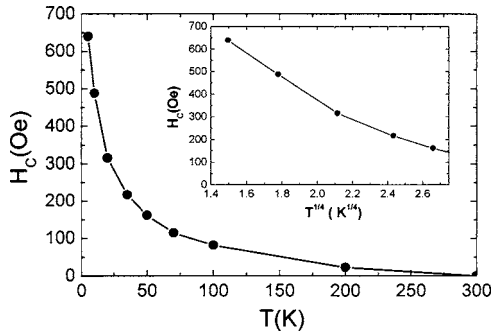
FIG. 8. The coercive field approximately scales as $T^{1/4}$ at low temperatures.

volume of the particle. The preexponential factor τ_0 also depends on E_{Ba} and E_{Bint}, i.e.,

$$\tau_0 = \frac{\sqrt{\pi}}{4} \frac{|\mu(0)|}{E_B \gamma_0} \left[\frac{1}{\eta_r} + \eta_r \left(\frac{\mu_{nr}(T)}{\mu_{nr}(0)} \right)^2 \right] \times \sqrt{\frac{kT}{E_B}} \left(1 + \frac{kT}{E_B} \right),$$

(2)

where $\mu(0)$ is the particle magnetic moment at 0 K, $\mu_{nr}(0)$ the corresponding nonrelaxing magnetization, γ_0 is the gyromagnetic ratio, and η_r is the reduced damping constant [$\eta_r = \eta \gamma_0 \mu_{nr}(0)$]. Thus τ, and hence T_B, depends on both the size (V) of the particles, as well as the interparticle interactions, and in the latter case with a more complex functional dependence. In the samples studied here, the particles are fairly monodispersed as indicated by the TEM and AFM images in Fig. 1(a). Therefore, since the particle size is relatively constant, it is likely that the distribution of blocking temperatures is due to the variation in interparticle interactions E_{Bint} that results from the random spacing of nearest neighbors across the sample. It is notable that Puntes *et al.*,[26] Hyeon *et al.*,[27] and Sun and Murray[28] also found broad blocking peaks on a regularly arranged two-dimensional superlattice of various monodispersed magnetic nanocrystals, where the size polydispersity would hardly contribute to the peak broadness.

Further, according to the theory of superparamagnetism,[22,29] rotation of the superparamagnetic spins in the presence of a field is thermally activated, provided kT is greater than E_{Ba}, the anisotropy energy. For a system of randomly oriented noninteracting identical particles, the coercivity is expected to follow the relation

$$H_c(T) = H_c(0) \left[1 - \left(\frac{T}{T_B} \right)^{1/2} \right],$$

where $H_c(0) = 0.64 K/M_s$, and K is the anisotropy constant. The plot of H_c vs T is given in Fig. 8 where it is noted that the above law, applicable for randomly oriented independent particles, is not exactly followed. It is rather found that exponent is ~1/4 up to a temperature 30 K, as shown in the inset. This is to be expected because of the interparticle interactions in our sample, as reflected in the ZFC curve. Several authors have reported that the $T^{1/2}$ power law only applies in a limited low-temperature range for interacting nanoparticle systems. For example, Fonseca *et al.*[22] observed that the law holds for temperatures up to ~16 K in a silica matrix with doped Ni particles. Sun and Dong[30] found that it

applied to graphite-encapsulated Ni/NiO particles up to ~120 K, and McHenry *et al.*[31] found it to hold for carbon-coated SmCo particles for temperatures up to ~25 K. Brunsman *et al.*[32] discovered that for the interacting Nd–Fe–B–C nanoparticles, the power law was obeyed with an exponent of 0.3 instead of 0.5. It appears from the above-cited reports that the noninteracting character of the particles is enhanced by a robust solid surface coating such as encapsulation of a graphite layer rather than a labile surfactant layer, because the latter still cannot shield the long-range dipolar forces among the particles.

IV. CONCLUSIONS

Ni nanoparticles produced by laser-driven pyrolysis of $Ni(CO)_4$ are, with proper parametric controls, very monodispersed and have clean surfaces with no evidence of oxidation. The dipolar interaction among the particles may be responsible for suppressing the independent character of the particles. This may entail the broadness of the blocking behavior while the field-temperature scaling in the superparamagnetic regime remains intact. In view of the fact that the crystal-field effects of ligands on the surface of the nanoparticles significantly affect the electronic structure of the former and alter the magnetic properties, these particles can serve as a good model system where different chosen ligands can be bound on the surface and magnetic properties systematically studied.

[1] M. P. Pileni, Adv. Funct. Mater. **11**, 323 (2001).
[2] D. L. Leslie-Pelecky and R. D. Rieke, Chem. Mater. **8**, 1770 (1996).
[3] R. Skomski, J. Phys.: Condens. Matter **15**, R841 (2003).
[4] P. N. Prasad, *Nanophotonics* (Wiley, New York, 2004).
[5] S. E. Apsel, J. W. Emmert, J. Deng, and L. A. Bloomfield, Phys. Rev. Lett. **76**, 1441 (1996).
[6] I. M. L. Billas, A. Chatelain, and W. A. de Heer, Science **265**, 1682 (1994).
[7] J. H. Vincent and P. S. Sangha, GEC J. Res. **13**, 2 (1996).
[8] C. B. Murray, S. Sun, W. Gaschler, H. Doyle, T. A. Betley, and C. R. Kagan, IBM J. Res. Dev. **45**, 47 (2001).
[9] N. Feltin and M. P. Pileni, Langmuir **13**, 3927 (1997).
[10] E. R. Leite, N. L. V. Carreño, E. Longo, A. Valentini, and L. F. D. Probst, J. Nanosci. Nanotechnol. **2**, 89 (2002).
[11] B. J. Jonsson, T. Turkki, V. Strom, M. S. El-Shall, and K. V. Rao, J. Appl. Phys. **79**, 5063 (1996).
[12] E. M. Gonzalez, M. I. Montero, F. Cebollada, C. de Jullian, J. L. Vincent, and J. M. Gonzalez, Europhys. Lett. **42**, 91 (1998).
[13] Y. He, X. Li, and M. T. Swihart, Chem. Mater. **17**, 1017 (2005).
[14] B. D. Cullity, *Elements of X-ray Diffraction*, 2nd ed. (Addison-Wesley, Reading, MA, 1978).
[15] R. A. Young, A. Sakthivel, T. S. Moss, and C. O. Paiva-Santos, J. Appl. Crystallogr. **28**, 366 (1995).
[16] L. Wu, H. J. Wiesmann, A. R. Moodenbaugh, R. F. Klie, Y. Zhu, D. O. Welch, and M. Suenaga, Phys. Rev. B **69**, 125415 (2004).
[17] M. P Morales, C. J Serna, F. Bødker, and S. Mørup, J. Phys.: Condens. Matter **9**, 5461 (1997).

[18]R. H. Kodama, A. E. Berkowitz, E. J. McNiff, Jr., and S. Foner, Phys. Rev. Lett. **77**, 394 (1996).

[19]V. Skumyrev, S. Stoyanov, Y. Zhang, G. Hadjipanayis, D. Givord, and J. Nogues, Nature (London) **423**, 850 (2003).

[20]Y. D. Yao, Y. Y. Chen, M. F. Tai, D. H. Wang, and M. H. Lin, Mater. Sci. Eng., A **217**, 837 (1996).

[21]R. H. Kodama, S. A. Makhlouf, and A. E. Berkowitz, Phys. Rev. Lett. **79**, 1393 (1997).

[22]F. C. Fonseca, G. F. Goya, R. F. Jardim, R. Muccillo, N. L. V. Carreno, E. Longo, and E. R. Leite, Phys. Rev. B **66**, 104406 (2002).

[23]D. Kechrakos and K. N. Trohidou, Appl. Phys. Lett. **81**, 4574 (2002).

[24]C. Liu and Z. J. Zhang, Chem. Mater. **13**, 2092 (2001).

[25]J. L. Dormann, L. Spinu, E. Tronc, J. P. Jolivet, F. Lucari, F. D'Orazio, and D. Fiorani, J. Magn. Magn. Mater. **183**, L255 (1998).

[26]V. F. Puntes, K. M. Krishnan, and P. Alivisatos, Appl. Phys. Lett. **78**, 2187 (2001).

[27]T. Hyeon, S. S. Lee, J. Park, Y. Chung, and H. B. Na, J. Am. Chem. Soc. **123**, 12798 (2001).

[28]S. Sun and C. B. Murray, J. Appl. Phys. **85**, 4325 (1999).

[29]C. P. Bean and J. D. Livingstone, J. Appl. Phys. **30**, 120S (1959).

[30]X. C. Sun and X. L. Dong, Mater. Res. Bull. **37**, 91 (2002).

[31]M. E. McHenry, S. A. Majetich, and E. M. Kirkpatrick, Mater. Sci. Eng., A **204**, 19 (1995).

[32]E. M. Brunsman, J. H. Scott, S. A. Majetich, M. E. McHenry, and M. Q. Huang, J. Appl. Phys. **79**, 5293 (1996).